

RHEOLOGICAL STUDY OF THE SOLIDIFICATION OF PHOTOPOLYMER AND DISPERSED NANOTUBE SYSTEMS

NONO DARSONO, HIROSHI MIZUNUMA, HIROMICHI OBARA

Department of Mechanical Engineering, Tokyo Metropolitan University,
1-1 Minamiohsawa Hachioji, Tokyo 192-0397, Japan

*Corresponding author: mizunuma@tmu.ac.jp

Fax: x81.42.6772701

Received: 17.5.2011, Final version: 11.8.2011

ABSTRACT:

We herein describe a set of rheological measurements that were carried out in order to characterize the solidification of photopolymers. The solidification depends on the length of time of exposure to UV light, and the intensity of that light, which reduces with distance from the irradiative surface. Liquid prepolymer was solidified inside the gap of a parallel disk rheometer by irradiation of the prepolymer with UV light through a fixed quartz disk. The rheological time-dependent changes were measured and analyzed for both unidirectional and oscillatory shear. The results were compared with those obtained by direct measurement in the absence of shear. When the thickness of the sample was less than 0.1 mm, the analysis for unidirectional shear flow yielded a reasonable agreement for both critical exposure and solidified depth. When the thickness was greater than 0.1 mm, the application of unidirectional shear delayed the start of the solidification but then caused it to occur more rapidly. This dependence of the solidification on the thickness of the sample was more significant for dispersed systems of nanotubes and for dynamic measurements made under oscillatory shear. The increase in viscosity due to photopolymerization was also estimated, and its effect was discussed.

ZUSAMMENFASSUNG:

Wir beschreiben eine Reihe von rheologischen Messungen, die durchgeführt wurden, um die Verfestigung von Photopolymeren zu charakterisieren. Die Verfestigung hängt von der Zeit, in der die Probe der UV-Strahlung ausgesetzt ist, und der Lichtintensität ab, die mit dem Abstand von der Strahlungsquelle abnimmt. Das flüssige Prepolymer wurde durch die Bestrahlung des Prepolymers durch eine feste Quarzscheibe im Spalt eines parallelen Platten-Rheometers verfestigt. Die zeitabhängigen rheologischen Änderungen wurden gemessen und analysiert sowohl für Scherung mit konstanter Schergeschwindigkeit als auch für oszillatorische Scherung. Die Resultate wurden mit denen verglichen, die durch direkte Messung ohne Scherströmung gewonnen wurden. Wenn die Probendicke kleiner als 0.1 mm ist, führt die Analyse der Ergebnisse für eine stationäre Scherströmung zu einer guten Übereinstimmung sowohl für die kritische Bestrahlung als auch für die Verfestigungstiefe. Wenn die Probendicke größer als 0.1 mm ist, verzögert die Anwendung einer Scherung mit konstanter Schergeschwindigkeit den Beginn der Verfestigung, führt danach jedoch zu einer beschleunigten Verfestigung. Diese Abhängigkeit der Verfestigung von der Probendicke war für disperse Systeme mit Kohlenstoffnanoröhrchen bedeutend bei dynamischen Messungen unter oszillatorischer Scherung. Die Zunahme der Viskosität aufgrund der Photopolymerisation wurde ebenfalls abgeschätzt und der Effekt diskutiert.

RÉSUMÉ:

Nous décrivons ici un ensemble de mesures rhéologiques qui ont été faites dans le but de caractériser la solidification de photopolymères. La solidification dépend de la durée d'exposition à la lumière UV et de l'intensité de cette lumière qui diminue avec la distance calculée depuis la surface irradiante. Un liquide pré-polymérique a été solidifié à l'intérieur de l'entrefer d'un rhéomètre équipé de disques parallèles en irradiant le pré-polymère avec une lumière UV à travers un disque de quartz. Les changements rhéologiques au cours du temps ont été mesurés et analysés en cisaillement oscillatoire et continu. Les résultats ont été comparés avec ceux obtenus par mesure directe en l'absence de cisaillement. Lorsque l'épaisseur de l'échantillon est inférieure à 0.1 mm, l'analyse en cisaillement continu conduit à un accord raisonnable pour l'exposition critique et la profondeur de solidification. Lorsque l'épaisseur est supérieure à 0.1 mm, l'application d'un cisaillement continu retarde le début de la solidification mais ensuite induit une solidification plus rapide. Cette dépendance de la solidification avec l'épaisseur de l'échantillon est plus importante pour les systèmes dispersés de nanotubes et pour les mesures dynamiques effectuées avec un cisaillement oscillatoire. L'augmentation de la viscosité associée à la photopolymérisation a aussi été estimée et son effet est discuté.

KEY WORDS: photopolymer, solidification, exposure, shear flow, nanotubes

1 INTRODUCTION

A photopolymer is composed of a monomer, an oligomer and a photoinitiator, and is generally solidified by ultraviolet (UV) light. The photosolidification of a prepolymer has a number of advantages in that it is fairly rapid and requires less energy than a thermal process, does not entail the use of organic solvents, and may be applied to a selected area by means of a masking technique [1, 2]. Photopolymers have been widely used in coating, printing and adhesives, and so on. These solidification characteristics are influenced by the presence of dispersed particles in the photopolymer. These insoluble additives are used to improve the properties of the photopolymer, including its mechanical strength and conductivity of heat or electricity. Bauer and Menhert [3] investigated the effect of nano-sized particles of silica on the properties of UV-curable acrylate, for example. They found that the addition of nanosilica improved the resistance of the acrylate coat to scratching and abrasion. Additives such as glass powder and carbon may also be used as fillers for the polymer composite. Such additives include carbon nanotubes (CNTs), which are well known to be an attractive material following their discovery by Iijima [4]. The mechanical, electrical, and rheological properties of the polymer and the CNT composites were reviewed by Moniruzzaman and Winey [5]. In order to optimize and control the solidification process of the dispersed system, it is important to clarify the influence of dispersion of these particles on the solidification.

In any material, the intensity of light $i(x)$ is reduced with depth x by absorption. The transmittance T may be expressed in terms of the ratio $i(x)/I_s$, where I_s is the intensity of the light irradiated from the surface of the material. The absorbance A is defined as $A = -\ln(i(x)/I_s)$, and is proportional to the depth of penetration x . This relationship is called Beer-Lambert law, and the intensity $i(x)$ at a given point in material is given by

$$i(x) = I_s / \exp(x/D_p) \quad (1)$$

where a constant D_p is a depth of penetration, and represents the depth at which the irradiance becomes $1/e$ times that at the surface. Photopolymers are subject to the Beer-Lambert law. In addition, solidification due to photopolymer-

ization begins above a critical level of exposure E_c , which represents the energy level at which the photopolymer changes from a liquid to a solid. The UV light is absorbed by the polymer. The exposure $e(x,t)$ in the polymer is given by $i(x)t$ at time t , and decreases with penetration depth x as

$$e(x,t) = I_s t / \exp(x/D_p) \quad (2)$$

The solidified depth $h(t)$ is that depth x at which $e(x,t)$ reaches the value E_c . By assuming that $e(x,t) = E_c$, $x = h$, and $I_s t = E_s$ in Equation 2, the depth may be represented by the working curve Equation 1

$$h = D_p \ln(E_s/E_c) \quad (3)$$

E_s is the exposure at the surface of the polymer. The process of solidification is therefore characterized by the constants E_c and D_p .

There are three methods of measurement of the constants E_c and D_p . These are (1) by direct measurement, (2) using a technique based on the detection of a chemical reaction, and (3) by a rheological method. The direct method is the simplest of these methods. In it, the liquid prepolymer is exposed to UV light. After exposure, the liquid phase is removed manually, and the thickness h of the remaining solidified polymer is measured. This measurement is repeated across a range of exposure, and a curve of h is plotted as a function of $\ln(E_s)$. The extrapolation of this semi-logarithmic plot crosses the line $h = 0$ at E_c , and the gradient yields the value of D_p . This method is commonly used, by virtue of its simplicity. However, the removal of the liquid phase must be done manually, and careful measurement is therefore necessary to determine the precise thickness of the solidified polymer.

In the second chemical method, the kinetics of the reaction are measured using differential scanning calorimetry (DSC) or real-time infrared spectroscopy (RTIR). Photo-DSC detects the heat of a reaction, and is used to analyze the photo-initiated reactions. RTIR is used to measure the absorption of different IR frequencies by a sample. Different functional groups absorb different characteristic frequencies of IR radiation, thereby allowing RTIR analysis to be used to determine the conversion of the selected functional group by means of real time spectroscopy. Castell et al.

[6] applied both these methods together with a rheological method, and showed that they were complementary in the characterization of photopolymerization.

The third method measures the changes in the rheological properties induced by solidification. In this method, a shear flow is produced between two parallel plates. UV light is irradiated from one plate into the prepolymer. Above the critical level of exposure, gelation begins on the irradiation surface, causing the photopolymer to become divided into a solid and a remaining liquid layer. The thickness of the liquid layer reduces, and the apparent viscosity increases, with increasing exposure time. Watanabe et al. [7] studied the rheological behavior of epoxy acrylate prepolymer during UV curing. They developed an oscillating plate rheometer, in which a shear flow was produced in the space between a fixed plate and a linearly oscillating one. UV irradiation of the prepolymer increased its dynamic viscosity. Using this rheometer, Otsubo et al. [8, 9] discussed the influence of sample thickness and non-homogeneous gelation on the dynamic viscosity. Khan et al. [10, 11] installed a UV light system into a rotating rheometer and irradiated UV light from one side of the parallel disks. After various exposure times, they extinguished the UV light and measured the dynamic moduli G' and G'' . Chiou et al. [12] used the same apparatus with Fourier transform mechanical spectroscopy, and measured the dynamic moduli in real time during solidification. In order to monitor a fast curable polymer system, Lee et al. [13] measured the strain-stress response, which was sampled at a rate of 200 points per second in a parallel plate rheometer. The wave forms thus obtained were analyzed to yield the time-dependence of the dynamic moduli. Schmidt et al. [14] increased the sampling rate of this method to 1000 points/s, and enabled to monitor the faster curable systems. Some commercial rheometers now include optional UV irradiation equipment. Thus, rheological measurement is a practical tool for the investigation of the solidification of photopolymers. However, all studies apart from that of Otsubo et al. [9] have assumed homogeneous gelation over the whole of the material. As suggested by Equation 3, solidification begins from the light irradiation surface and the rheological properties depend on the distance from the surface.

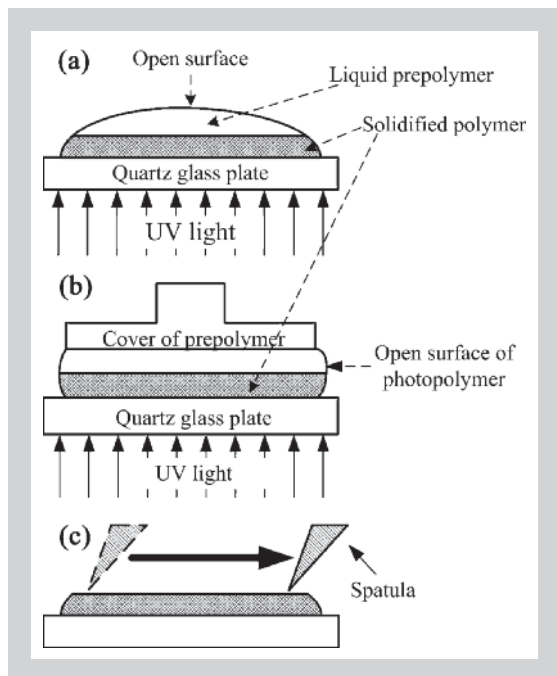
We herein discuss a method of characterization that considers the co-existence of liquid and solid layers during solidification. UV light penetrates the liquid prepolymer, thereby starting the process of photopolymerization from the irradiation surface. The solidification is not only time-dependent but also dependent on the depth of light penetration. These solidification characteristics were investigated for both unidirectional and oscillatory shear. Since the rate of solidification was fairly rapid, the initial pre-gel state was assumed to turn to the post-gel state instantaneously. The effects of shear, sample thickness, and suspended nanotubes were investigated, and the results were compared with those obtained by direct measurement. The influence of increasing viscosity prior to solidification was also estimated and discussed.

2 EXPERIMENTAL METHODS

2.1 MATERIALS AND RHEOLOGICAL CHARACTERIZATION

The photopolymer used in our experiments was a pale yellow prepolymer (Afit UAP-75). Its main components were 2,2-bis[4-(acryloxy diethoxy)phenyl]tricyclodecane dimethanol diacrylate, and a thickener. The photoinitiator was a mixture of Irgacure 184 and 819, the concentration of which was 1%. The filler was composed of single-walled carbon nanotubes (CNTs), supplied by Nikkiso Co., Ltd. The diameter and the length of the nanotubes were typically 2 nm and a few microns, respectively. These CNTs were produced by a Direct Injection Pyrolytic Synthesis, which is a type of Chemical Vapor Deposition method. CNTs in the form of bukypaper were initially dispersed in acetone using an ultrasonicator (Branson Sonifier 150) for 12 hours. In order to prevent the evaporation of the acetone, the temperature was maintained at between 0 and 4°C by means of a temperature control bath during ultrasonication. The sonicated CNTs were dried in a convection oven at 70°C, and then mixed with the prepolymer for one hour. Prepolymers with CNTs of 0.05 and 0.1 wt% were prepared for the measurements.

The steady shear and dynamic complex viscosities were measured using a cone and a plate rheometer (Thermo Haake RS 600). The cone diameter was 20 mm and the gap angle was 1°.



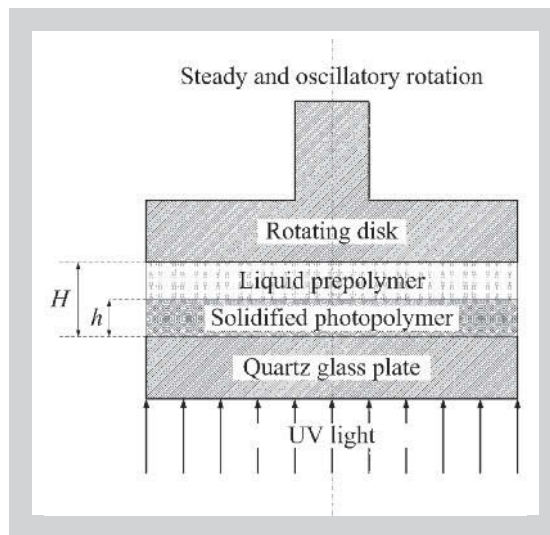
The dynamic measurement was carried out under a control stress mode of 5 Pa.

2.2 DIRECT MEASUREMENT OF SOLIDIFICATION CHARACTERISTICS

The liquid prepolymer was put on a quartz glass plate, through which UV light (Sumita LS-165 UV) was irradiated, as shown in Figure 1a. The UV light was UVA, and the peak wave length was 365 nm. The surface intensity I_s of the UV light was measured at the glass surface. Since the presence of oxygen in the prepolymer inhibits the photopolymerization, its diffusion from the air into the prepolymer through the open surface may suppress the solidification. This possibility was investigated by covering the prepolymer with a plate, as shown in Figure 1b. In this case, the open surface was limited to the small gap. After an exposure time t the irradiation was stopped, and the liquid part was removed using a spatula, as shown in Figure 1c. The thickness h of the solid part was then measured. This process was repeated for a number of different exposure times. Surface exposure E_s was obtained using $E_s = \text{surface light intensity } I_s \times \text{exposure time } t$, and a working curve of h against $\ln(E_s)$ was then plotted. The gradient of the semi-logarithmic plot yielded the depth of penetration D_p from Equation 3, and the extrapolation of the curve to $h = 0$ yielded the critical exposure E_c .

2.3 RHEOLOGICAL MEASUREMENT OF SOLIDIFICATION CHARACTERISTICS

The unidirectional shear and dynamic complex viscosities were measured using a parallel disk rheometer (Thermo Haake RS 600), as shown in Figure 2, in which UV light was irradiated into the



liquid prepolymer through a light guide made of quartz glass fibers. The rotating aluminum disk was disposable. In order to study the influence of the sample thickness on solidification, the experiments were conducted for a disk gap of 0.025 to 0.4 mm. The temperature was maintained at a constant 25°C. A pre-shear of 5 s was applied to ensure the stabilization of the sample prior to irradiation with UV light. Above the critical exposure E_c , solidification began from the quartz glass surface, and the thickness of the solid layer on the glass plate gradually increased.

The depth dependence of the solidification was caused by that of the reduction of the transmitted light, as given by Equations 1 and 2. This dependence on depth is somewhat at odds with the homogeneity of chemical gelation. Homogeneous gelation has previously been investigated rheologically through measurements of dynamic viscoelasticity, from which a gel point has been predicted. Tung and Dynes [15] and Winter [16, 17] proposed rheological methods of detection of the gel point. As discussed in our introduction, gelation of photopolymers was investigated using the same rheological methods as for homogeneous gelation. However, the same methodology is not appropriate for photosolidification. An alternative approach is introduced herein that is based on the following assumptions:

- The photopolymer is divided into two layers of liquid and viscoelastic solid between the parallel disks. The thickness of each layer varies during solidification.
- In the unidirectional measurement of shear, the viscous property of the liquid layer does not change prior to solidification, and the viscosity of the initial prepolymer is preserved.
- In dynamic complex measurement, the values of the moduli G'_l and G''_l of the initial liquid layer, and of the moduli G'_s and G''_s of the solidified layer, are preserved during solidification.

Figure 1 (left): Direct measurement of solidification characteristics. The prepolymer surface was open in (a) and covered with a disk in (b) in order to minimize contact with oxygen. After UV light was extinguished in (c), the upper liquid prepolymer was removed using a spatula, and the thickness of the solidified photopolymer was measured.

Figure 2: Solidification in the parallel disk rheometer.

The first of the foregoing assumptions is consistent with the process of the photo-solidification. The second assumption accounts for the rapid change from liquid to solid, because photopolymerization is generally faster than other kinds of chemical gelation. However, there is a possibility that exposure of the prepolymer to light in the region of E_c may induce a non-negligible increase in viscosity. The usefulness and limitations of the foregoing assumptions are discussed in the next section.

In the case of unidirectional shear, the characterization may be formulated as follows:

Step I: Shear rate $\dot{\gamma}(M)$: In this step the shear rate $\dot{\gamma}$ is defined to be a function of the moment M at the rim of the disk. The shear rate $\dot{\gamma}$ is $R\omega/H$, where R is the radius of the disk, ω is the angular velocity, and H is the distance between the disks. First, we measure M as a function of the shear rate $\dot{\gamma}$, such that the inverse function of $M(\dot{\gamma})$ is obtained as follows

$$\dot{\gamma} = \dot{\gamma}(M) \quad (4)$$

At this stage, a rheological model of the liquid prepolymer is not necessary. However, if the rheological model is known, we can deduce the shear rate $\dot{\gamma} = \dot{\gamma}(M)$ to be a function of M . In a parallel disk viscometer, the torque moment M is

$$M = 2\pi \int_0^R \tau_r r^2 dr = \frac{2\pi R^3}{\dot{\gamma}^3} \int_0^{\dot{\gamma}} \tau_r \dot{\gamma}_r^2 d\dot{\gamma}_r \quad (5)$$

where τ_r and $\dot{\gamma}_r$ are the shear stress and shear rate at the radial coordinate r . The parallel disk rheometer can be used to measure a non-Newtonian viscous property [18]. In the case of Newtonian fluid, $\tau = \eta\dot{\gamma}$, and $M(\dot{\gamma}) = \pi R^3 \eta \dot{\gamma} / 2$ from Equation 5. Then

$$\dot{\gamma}(M) = \frac{2}{\pi R^3 \eta} M \quad (6)$$

Step II: Solidified depth h : For an angular velocity ω and a surface light intensity I_s , continuous UV irradiation increases the exposure in the photopolymer. The light intensity in the photopolymer is highest at the irradiation surface, at which the exposure approaches the critical

exposure E_c prior to the start of solidification. The depth of prepolymer that has been exposed to E_c increases with time. This process of solidification reduces the thickness of the liquid layer and increases both the shear rate $\dot{\gamma}$ and the torque moment, M . Both the measured moment M and Equation 4 provide the value of $\dot{\gamma}$, which is equal to $R\omega/(H-h)$ at the rim of the disk. Thus, the solidified depth h is obtained from

$$\frac{h}{H} = 1 - \frac{R\omega}{\dot{\gamma}(M)H} \quad (7)$$

In the case of a Newtonian fluid, the moment M_o at the start of exposure to UV is defined by $M_o = (\pi R^3 \eta / 2)(R\omega/H)$ and from Equations 6 and 7

$$\frac{h}{H} = 1 - \frac{M_o}{M} \quad (8)$$

Step III: Critical exposure E_c and depth of penetration D_p : The solidified depth h is plotted as a function of the exposure E_s . The critical exposure E_c is determined by the appearance of an increase in h that signifies the start of the solidification. The gradient of the curve of h against $\ln(E_s/E_c)$ gives the depth of penetration D_p , as defined by Equation 3.

The measurement was performed under the controlled shear rate mode of the software of the rheometer. The initial shear rate was 100 s^{-1} . This operational mode sets a constant angular disk velocity. Once critical exposure has been obtained in the solidification measurements, the shear rate is further increased, as discussed above. Measurements were ceased when the shear stress reached 127 kPa. For the dynamic complex measurements, the characterization as formulated as follows.

Step I: Complex moduli: The apparent moduli G'_{ap} and G''_{ap} were measured under a constant angular frequency ω . The incidence of UV irradiation increased the moduli above the critical level of exposure. These increases in the moduli are caused by an increase in the fraction of the solid layer, which has larger moduli than the liquid layer. The moduli G'_l and G''_l are defined as the moduli G'_{ap} and G''_{ap} before UV irradiation, and the moduli G'_s and G''_s are defined as the moduli G'_{ap} and G''_{ap} after full

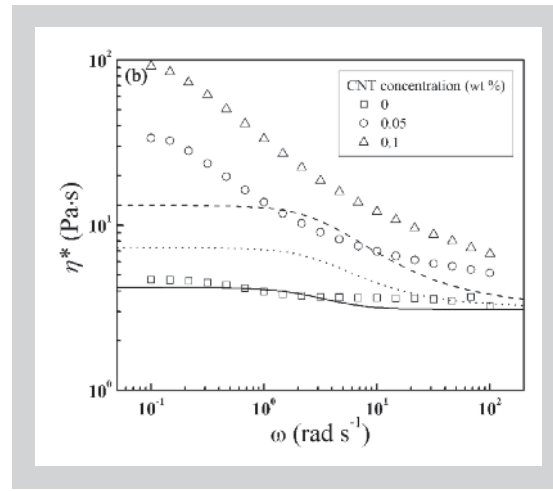
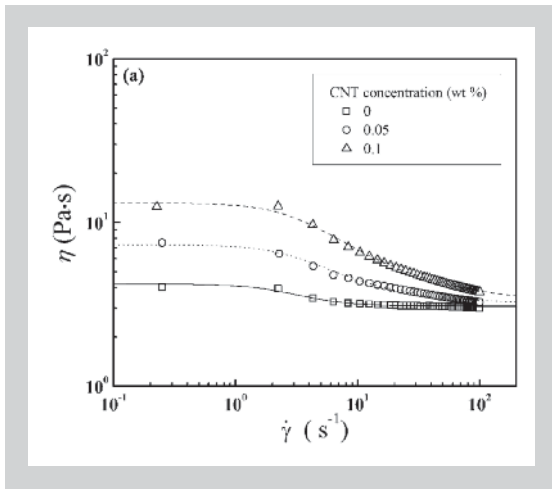


Figure 3: Viscous properties of prepolymer and CNT dispersed systems. (a) Steady shear viscosity as a function of shear rates. (b) Complex viscosity as a function of frequency. The Carreau model curves were fitted using steady shear viscosity.

Table 1: Model constants obtained from steady shear measurements.

solidification. Moduli with the subscripts *l* and *s* correspond to those of the liquid and solid layers, respectively.

Step II: Solidified depth *h*: The apparent moduli G'_{ap} and G''_{ap} obtained from the rheometer are approximated by linear combinations of the moduli of the liquid and solid layers as follows.

$$G'_{ap} = G'_l \frac{H-h}{H} + G'_s \frac{h}{H} \quad (9)$$

$$G''_{ap} = G''_l \frac{H-h}{H} + G''_s \frac{h}{H} \quad (10)$$

By assuming that $G'_l \ll G'_s$ and $G''_l \ll G''_s$, the storage moduli and loss moduli give the solidified depth *h* as follows.

$$\frac{h}{H} \cong \frac{G'_{ap} - G'_l}{G'_s} \quad (11)$$

or

$$\frac{h}{H} \cong \frac{G''_{ap} - G''_l}{G''_s} \quad (12)$$

Step III: The critical exposure E_c and the depth of penetration D_p were obtained in the same way as for Step III for the case of unidirectional shear mentioned above. The measurements were performed under a controlled stress mode of 50 Pa, and the oscillatory frequency was fixed at 1 Hz.

3 EXPERIMENTAL RESULTS AND DISCUSSION

3.1 RHEOLOGICAL CHARACTERISTICS

The rheological characteristics were measured using a cone and a plate rheometer, as mentioned in Section 2.1. Figure 3a shows the shear

viscosity η as a function of shear rate. The prepolymer shows weak shear thinning, and dispersed systems demonstrate an increase in shear thinning with concentration. Newtonian plateaus appear at shear rates lower than 1 s^{-1} and higher than 10^2 s^{-1} . In order to express this shear thinning property of CNT dispersions, Kharchenko et al. [19] and Rahatekar et al. [20] used Carreau and Cross models, respectively. Ma et al. [21] applied a Fokker-Planck based orientation model for dispersed CNTs, and described the shear thinning viscosity and linear viscoelasticity of the dispersed system. In the present study, the viscosity curves in Figure 3a are fitted by the Carreau model

$$\eta = \eta_\infty + \frac{\eta_0 - \eta_\infty}{\left\{1 + (\dot{\gamma}/C)^2\right\}^n} \quad (13)$$

where η_0 is the limiting viscosity at zero shear rate, and η_∞ is the limiting viscosity at an infinite shear rate. *C* and *n* are the model constants. The constants used in the curves of Figure 3a are shown in Table 1. The Carreau model fitted the experimental results rather better than the Cross model.

The complex viscosity η^* is shown in Figure 3b, together with the Carreau model curves for steady shear viscosities η . The prepolymer obeys the Cox-Merz rule in that the complex viscosity of the prepolymer showed a good correlation with the shear viscosity. The dispersed systems, however, showed more significant shear thinning in the dynamic measurements. This failure of the Cox-Merz rule was observed by Kinloch et

CNT concentration (wt%)	Steady shear Carreau model			
	η_0	η_∞	<i>C</i>	<i>n</i>
0	4.41	3.10	3.03	1.03
0.05	7.31	3.20	3.03	0.48
0.1	13.1	3.26	3.03	0.41

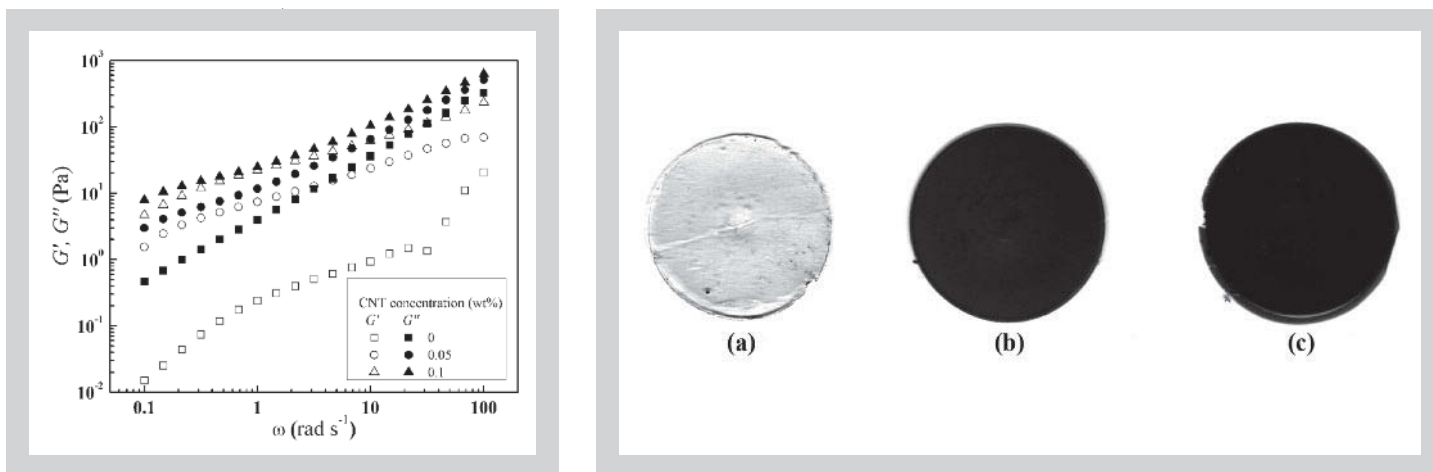
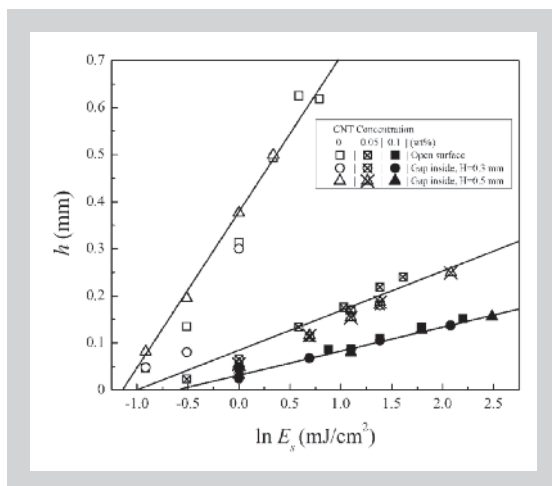


Figure 4 (left above): Storage modulus G' and loss modulus G'' as a function of frequency for prepolymer and CNT dispersed systems.

Figure 5 (right above): Solidified photopolymer under a steady shear flow between two parallel disks. The CNT concentrations are (a) 0 wt%, (b) 0.05 wt% and (c) 0.1 wt%. The gap between the disks was 0.1 mm.

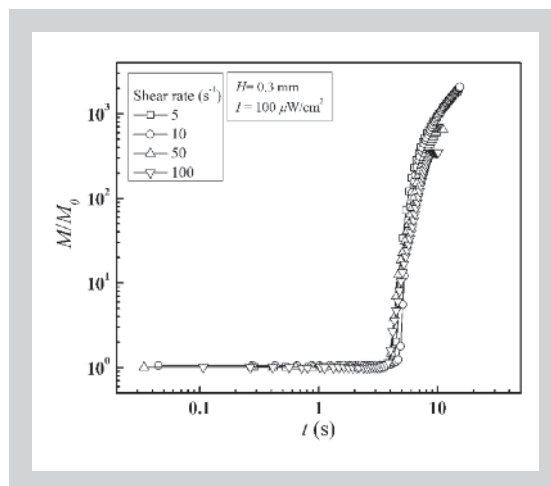
Figure 6 (left below): Solidified depth measured by the direct method. The UV light intensity was 200 $\mu\text{W}/\text{cm}^2$.

Figure 7 (right below): Influence of shear rate on the time-dependent increase in torque moment. The distance between the disks H was 0.3 mm and the UV light intensity was 100 $\mu\text{W}/\text{cm}^2$. The sample used was a prepolymer without CNT.



al. [22] and Fan and Advani [23] for CNT dispersions. Figure 4 shows the storage modulus G' , and the loss modulus G'' , for both the prepolymer and CNT dispersions. Whilst the addition of CNTs into the prepolymer significantly increases G' , there is only a modest increase in G'' . These changes in G' and G'' are consistent with results obtained previously by Pötschke et al. [24] and Ma et al. [21] for CNT dispersions.

Ma et al. [25] observed microscopic aggregate structures of CNTs in a shear flow for dispersion of untreated CNTs. By contrast, however, they observed a uniform dispersion for treated CNTs. In the present study, the dispersed systems that solidified under a unidirectional shear flow showed a uniform dispersion (see Figure 5), and the aggregate structures were not observed. The viscoelastic properties of CNT dispersed systems have been investigated by a number of different researchers. As discussed by Fan and Advani [23] the properties depend on the method of dispersion, the aspect ratio of the CNTs, the concentration, and the interaction between the CNTs. As mentioned above, the dispersed systems described herein have rheological properties that are in common with some other reported results, and are considered to have characteristics that are rheologically normal.



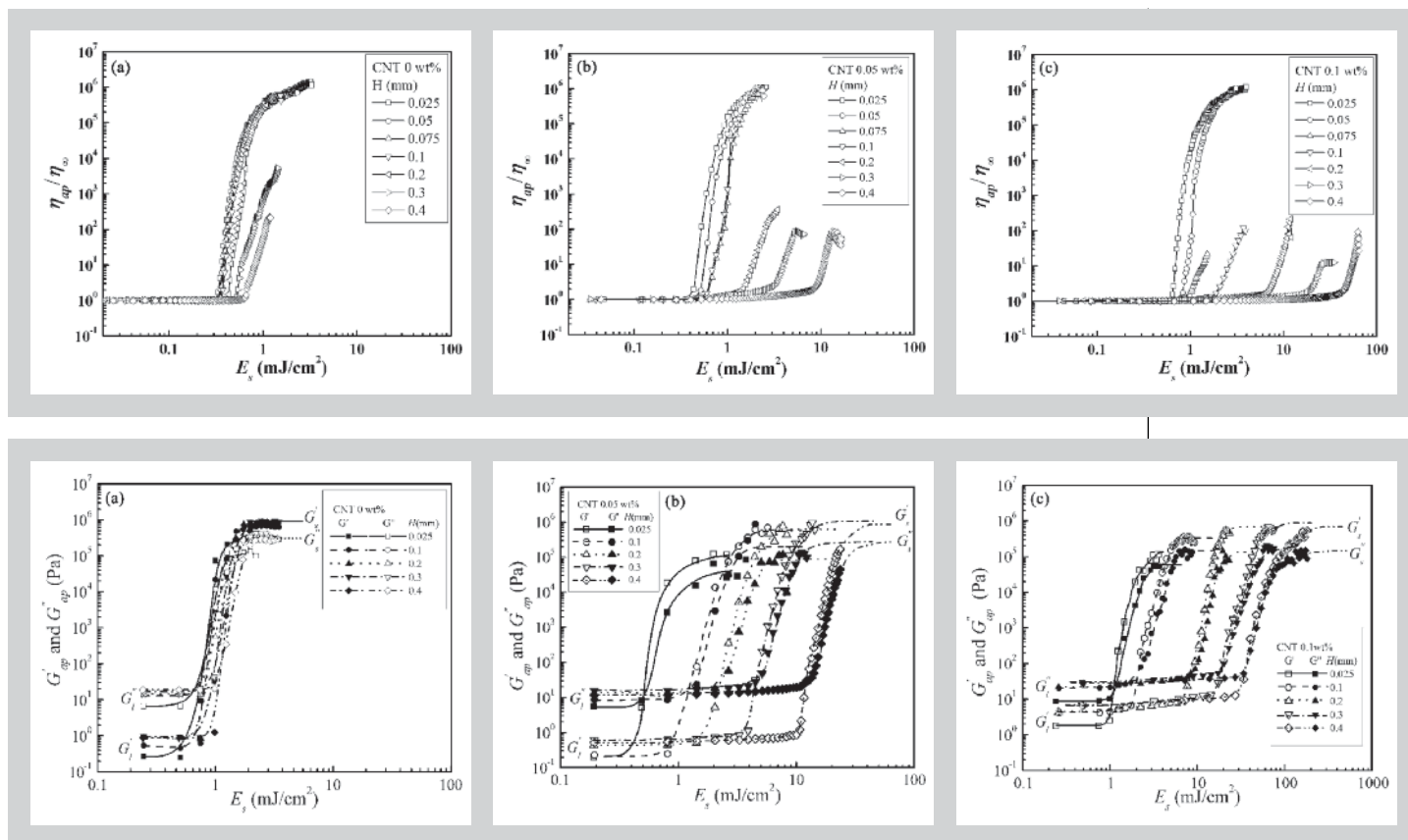
3.2 DIRECT MEASUREMENTS OF SOLIDIFICATION CHARACTERISTICS

Figure 6 shows the solidified depth h that was measured for the photopolymer and CNT dispersions. The sample surface was either open to the air, or covered with a disk. The thickness of the covered sample was adjusted to 0.3 or 0.5 mm. Oxygen was allowed to diffuse into the prepolymer through the open surface, thereby suppressing photopolymerization. However, the solidification was not influenced by the difference in the area of contact between the sample and air. We may therefore ignore the effect of the oxygen in the air in our experiments. The solidification depth h increases linearly against $\ln(E_s)$, and therefore obeys Equation 3. The gradient of the curve gives the depth of penetration D_p , and extrapolation to $h = 0$ gives the critical exposure E_c . The dispersion of CNTs increases E_c and decreases D_p , due to the suppression of the penetration of light.

3.3 RHEOLOGICAL MEASUREMENTS OF SOLIDIFICATION CHARACTERISTICS

3.3.1 Time-dependent rheological behavior

We first investigated the influence of shear rate on solidification for unidirectional shear flow. In



this section, all rheological measurements were carried out using a parallel plate geometry, as mentioned in Section 2.3. Three initial shear rates of 10, 50, and 100 s⁻¹ were applied in the solidification experiments. Figure 7 shows the time-dependent increase in the non-dimensionalized moment M/M_0 , which is related to h/H by Equation 8. The time $t = 0$ corresponds to the incidence of UV light, and the pre-shear began five seconds before $t = 0$. Measurements were made up to a shear stress of 127 kPa and then stopped, in order to prevent overload of the sensor, as described in Section 2.3. Measurements at higher shear rates reached this limit earlier than those with a lower shear rate. Figure 7 shows that the shear rate influenced neither the critical exposure time, nor the ensuing initial increase in torque moment. In the present study, an initial shear rate of 100 s⁻¹ was applied to the measurements for unidirectional shear. As shown in Figure 3a, the effect of shear thinning on viscosity was approximately negligible at this shear rate.

Figure 8a shows the apparent viscosity η_{ap} as a function of surface exposure $E_s(t)$ for the photopolymer without CNTs. The disk distance H was varied in the range 0.025 - 0.4 mm. The surface exposure was $E_s(t) = I_s \times t$ where UV irradiation began at $t = 0$. Since the surface light intensity I_s was constant, Figure 8 shows the time-dependent change in apparent viscosity. Photoinitiated polymerization is generally influenced by not only the exposure but also the light intensity [26 - 28]. The

light intensity was kept constant hereafter, and thus we considered only the change of exposure due to the increase in time. The influence of the light intensity is out of scope in this study. The viscosity measurements were obtained from the rheometer software, which assumed that the material had a constant thickness H throughout the measurements. Before UV irradiation, the viscosity of the prepolymer was approximately η_∞ at the shear rate of 100 s⁻¹. The apparent viscosity increases after the start of solidification, at the critical exposure. Figure 8a indicates that this critical exposure is constant for small gaps in the range 0.025 to 0.1 mm. By contrast, for gaps larger than 0.1 mm, critical exposure increases with H . This dependence of critical exposure on H was more noticeable for the dispersed system of CNTs, as shown in Figures 8b and c. When the gap H was larger than 0.1 mm, the increase in viscosity was initially gradual, but then became rapid.

Figure 9 shows the values of G'_{ap} and G''_{ap} obtained from the dynamic measurements, as functions of $E_s(t)$. The initial liquid prepolymer had a higher loss modulus G''_{ap} than storage modulus G'_{ap} , and exposure increased G'_{ap} more significantly than G''_{ap} . These time-dependent changes in the storage and loss moduli have been investigated for homogeneous gelation by a number of different researchers. Tung and Dynes [15] proposed a definition of the chemical gel point to be the time of modulus crossover $G' = G''$. Winter and Chambon [16] and Winter [17]

Figure 8 (above): Non-dimensionalized changes in apparent viscosity as a function of exposure E_s . The change in the exposure $E_s = I_s \times t$ was equivalent to the change in t , because the light intensity I_s was maintained at a constant 200 $\mu\text{W}/\text{cm}^2$.

Figure 9: Variation of storage modulus G' and loss modulus G'' with exposure E_s . The light intensity I_s was maintained at a constant 200 $\mu\text{W}/\text{cm}^2$.

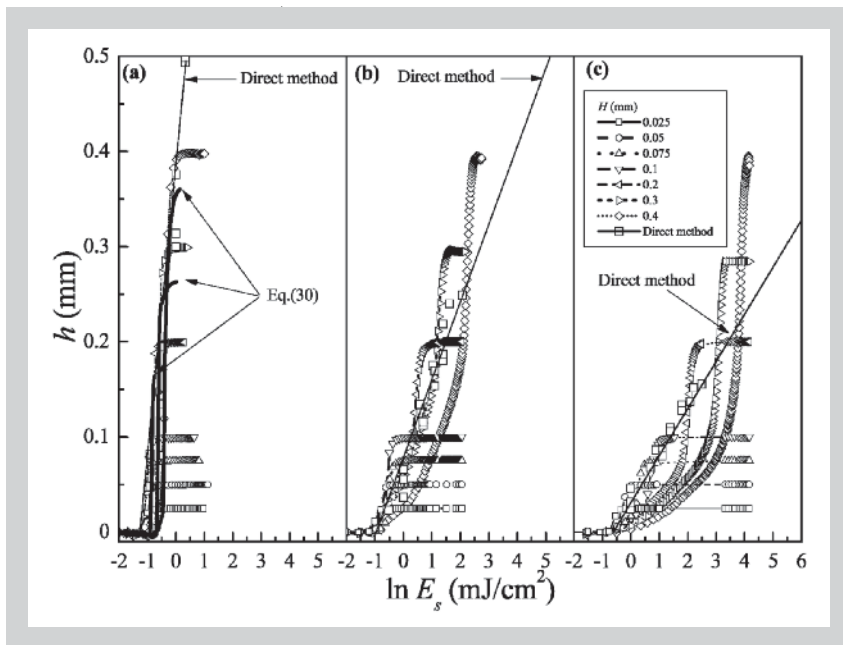


Figure 10: Variation of solidified depth h for unidirectional shear. The CNT concentration was 0% in (a), 0.05% in (b), and 0.1% in (c).

showed that the dynamic moduli follow a power law at the gel point. These rheological methods for the detection of the gel point were applied to photopolymers by Chiou et al. [12] and Lee et al. [13]. The moduli in Figure 9 indicate a similar crossover of G' and G'' . However, it remains unclear whether the detection of the gel point for homogeneous gelation may also be applied to depth-dependent gelation. Otsubo et al. [8, 9] investigated the influence of sample thickness in the range 0.004 - 0.2 mm by means of an oscillating plate rheometer. It can be seen that the moduli in Figure 9 shift to higher exposure with increasing H . Otsubo et al. [8, 9] observed a similar shift in dynamic viscosity. In our case, the dispersed systems showed a more significant shift to higher exposures.

3.3.2 Solidified depth h and critical exposure E_c

In the calculation of solidified depth h , the function $\dot{\gamma}(M)$ and the complex moduli must be given for Equations 7, 11, and 12. The function $\dot{\gamma}(M)$ may be obtained as the inverse function of $M(\dot{\gamma})$, which is calculated from Equation 5. As mentioned in Section 3.1, both the prepolymer and the dispersed systems obey the Carreau model of Equation 13. Since $\tau_r = \eta\dot{\gamma}_r$ in Equation 5, the Carreau model gives

$$M(\dot{\gamma}) = \frac{\pi R^3 \eta_\infty}{2} \dot{\gamma} \left(1 + \frac{\eta_o - \eta_\infty}{\eta_\infty} \left(\frac{C}{\dot{\gamma}} \right)^4 \frac{1}{(2-m)(1-m)} \times \left[1 - \left\{ 1 + \left(\frac{\dot{\gamma}}{C} \right)^2 \right\}^{1-m} \left\{ 1 - (1-m) \left(\frac{\dot{\gamma}}{C} \right)^2 \right\} \right] \right) \quad (14)$$

Although the function $\dot{\gamma}(M)$ is not expressed explicitly, $\dot{\gamma}$ may be calculated numerically by

inserting the given value of M on the left hand side of the above equation. In the unidirectional shear experiments, the initial shear rate was 100 s^{-1} and the shear rate increased with solidified depth. In this range of shear rates, the viscosity was approximately $\eta \cong \eta_\infty$ as shown in Figure 3a. The prepolymer that included the dispersed systems could therefore be assumed to be a Newtonian fluid with a constant viscosity η_∞ , and Equation 8 was applied to calculate the solidified depth h .

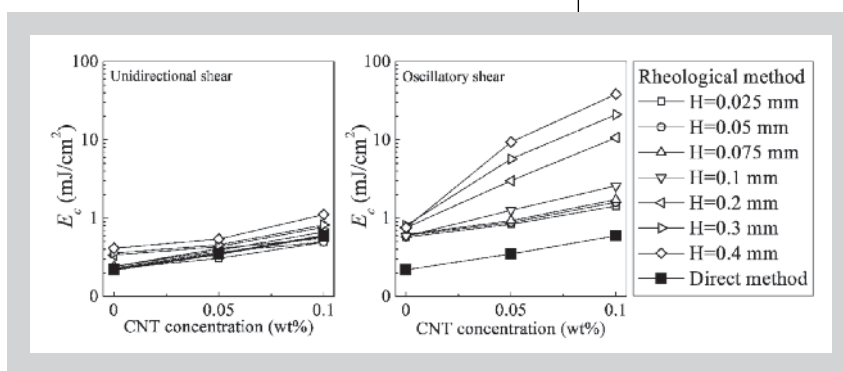
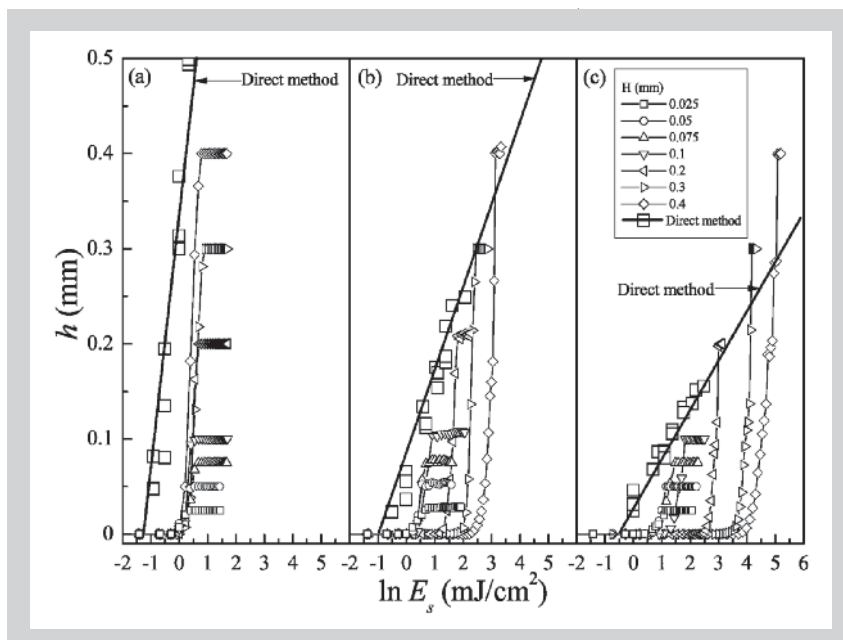
Figure 10 shows the calculated h as a function of $\ln(E_s)$ with the results of the direct measurements. At the end of the measurements, the rheometer automatically stopped the rotation of the disk because of the excess of moment above the prefixed upper limit. This corresponds to the change in h in Figure 10 from an increase to a plateau. The prepolymer without CNTs showed a solidification that was quite rapid compared with the dispersed systems. As shown in Figure 10a, a low value of H of up to 0.1 mm gives reasonable agreement with the solidified depth h that was obtained by direct measurement. On the other hand, when H was above 0.1 mm, the critical exposure increased, and there was also a faster increase in h .

In the dispersed systems, the increase in the solidified depth h could be divided into two stages, namely an initially slow solidification followed by a more rapid solidification, as shown in Figures 10b and c. These two stages correspond to the slow and fast increase of η_{ap} shown in Figures 8b and c. The initially low solidification rate was significant for the CNT dispersion of 0.1%, where an increase in solidified depth h was slowed down by an increase in gap width H . By contrast, the increasing rate of the second faster solidification was approximately independent of both H and the concentration of CNT.

The initial gradual increase in η_{ap} shown in Figures 8b and c was partially caused by the non-dimensionalization of viscosity in the vertical axis. In other words, if we assume a Newtonian fluid, the measured moment was initially $M_o = (\pi R^3 \eta_\infty / 2)(R\omega/H)$ and then $M = (\pi R^3 \eta_{ap} / 2)(R\omega/H)$. From these moments and Equation 8 the non-dimensionalized shear viscosity was $\eta_{ap} / \eta_\infty = M / M_o = 1 / (1 - h/H) \cong 1 + h/H$ for small h/H . In addition, h was proportional to $\ln(E_s)$ as indicated by Equation 3. Thus, the plot of η_{ap} / η_∞ against E_s indicates a slower increase for larger values of H . However,

this influence of H cannot explain the significant deviation from the results of direct measurement as shown in Figures 10b and c. In contrast with the rheological results, the direct measurement method did not indicate any influence of H on solidification, as shown in Figure 6. It is therefore suggested that the effect of H in the rheological measurements may be caused by flow shear.

Figure 11 shows the solidified depth h calculated from Equation 11. Equation 11 is related to the change in the storage modulus from G'_l to G'_s . The results, which were calculated from the loss modulus of Equation 12, indicate almost the same as those shown in Figure 11. These findings on the storage modulus are therefore discussed here. The most significant part of Figure 11 is the increase in the critical exposure. The total exposures for full solidification are not significantly different from the results of the direct measurements, but Figure 11 indicates a delay of the start of solidification in all cases. This delay corresponds to the initial gradual increase in G'_{ap} shown in Figure 9. The initial gradual increase in η_{ap} appears similarly in Figure 8, but the calculated h in Figure 10 does not show the significant increase in critical exposure shown in Figure 11. This difference is caused by the difference between Equations 8 and 11. The increase Δh in h may be approximated by $\Delta M/M_0$ in Equation 8 and by $\Delta G'_{ap}/G'_s$ in Equation 11. That is, Equation 8 predicts Δh to be caused by an increase in moment from the initial moment M_0 . By contrast, Equation 11 predicts Δh to be the ratio of the modulus increase $G'_{ap} - G'_l$ to the final modulus G'_s . In other words, Equation 8 uses the change of the shear rate in the liquid layer due to the growth of the solid layer, and Equation 11 uses the change of the material constant. The first, shear rate, method uses a simple shear flow, and it would therefore be possible to improve the precision of the measurement for the characteristics of solidification. The disadvantage of the first method is that the measurements must be stopped before full solidification occurs because of the divergence in viscosity. The second, material constant, method can be applied up to the end of full solidification, and the changes in the viscoelastic properties provide useful information about the material. However, in this second method, a more precise technique would be necessary for simultaneous characterization of the non-homogeneous solidification and the viscoelasticity.



The critical exposure E_c defined to be the exposure at which h increases in Figures 10 or 11, was plotted as a function of CNT concentration in Figures 12a and b. Figure 12a shows E_c for the unidirectional shear flow. An increase in the concentration of CNTs lowers transparency, as shown in Figure 5, and increases E_c . The rheological and direct methods give reasonable agreement on the critical exposure for a small gap of $H = 0.025 - 0.1$ mm. For a gap larger than 0.1 mm, the rheological method gives higher values of E_c than direct measurement. The higher exposure E_c obtained for a large H is correlated with the initial gradual increase in h shown in Figure 10. Figure 12b shows E_c for the oscillatory shear flow. The critical exposure E_c obtained by the rheological method is significantly higher than that obtained from the direct measurement, as suggested by Figure 11. A similar dependence of E_c on H was observed by Otsubo et al. [9]. They developed an oscillating plate rheometer with a plate distance of $H = 0.004$ to 0.2 mm, and measured the dynamic viscosity under UV exposure. The dependence of E_c on H that we observe here is therefore considered to be a general characteristic of the rheological measurement of photopolymerization.

Figure 11 (above): Variation of the solidified depth h for the dynamic measurements. The CNT concentration was 0 % in (a), 0.05 % in (b), and 0.1 % in (c).

Figure 12: Critical exposure as a function of CNT concentration.

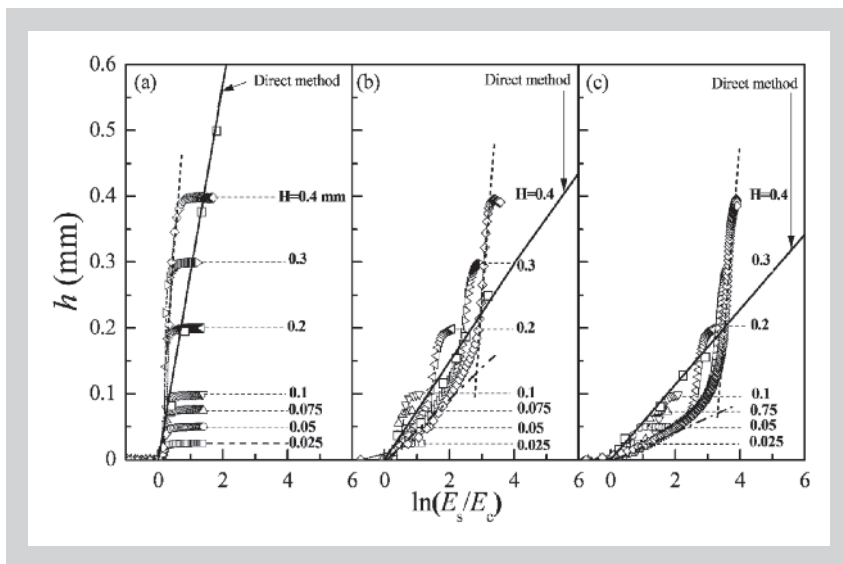
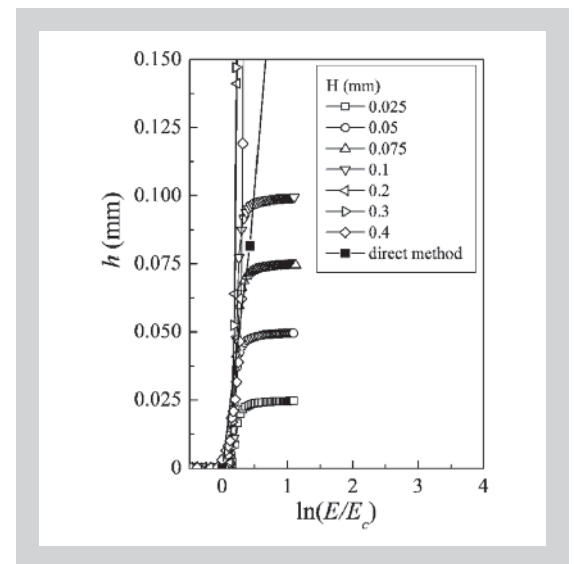


Figure 13 (left): Solidified depth h as a function of $\ln(E_s/E_c)$ for unidirectional shear. The CNT concentration was 0% in (a), 0.05% in (b), and 0.1% in (c).

Figure 14: Evolution of the solidified depth h near the glass surface for unidirectional shear. The CNT concentration was 0%.

Another characteristic parameter of solidification is the depth of penetration D_p , which is obtained from the gradient of Figures 13 to 15. In direct measurement, the solidified depth h is proportional to $\ln(E_s/E_c)$, as shown in Figure 6. For unidirectional shear flow without CNTs (Figure 13a), the rheological results for h up to 0.1 mm agree with the results from direct measurement. The results for h up to 0.15 mm are plotted in Figure 14. When the calculated h is higher than 0.1 mm, the rheological results show a higher solidified depth h than that found by direct measurement. Two possible reasons for this higher value of h are (1) the flow shear speeds up the photopolymerization reaction, which then enlarges the increase in h and (2) the increase in viscosity prior to solidification causes an overestimate of h . The second viscosity increase, which was neglected in the calculation of h here, is discussed in Section 3.5. The dispersed systems show, in Figures 13b and c, that the increase in h is divided into two stages from an initial gradual solidification to a subsequent rapid solidification.

In Figure 15 the solidified depth h obtained from the dynamic measurements is plotted as a function of $\ln(E_s/E_c)$. The results shown in Figure 11 were shifted by $\ln(E_c)$ in Figure 15. The shifted data were collapsed into a curve, the gradient of which is more or less independent of CNT concentration. The influence of the concentration appears to affect only E_c as shown in Figure 12b. Because this difference from the direct measurements was caused by shear flow, it is suggested that shear flow influences the reaction kinetics of the photopolymer. Khan [11] investigated the effect of shear on the gelation of photopolymers, and inferred from dynamic measurements that gelation was enhanced by shear. In our dispersed system, the initial rate of solidification was reduced, as mentioned above. CNTs are generally supposed to align their axes along the direction of shear, as observed by Pujari et al.



[29] and to suppress the penetration of light. On the other hand, the alignment of CNTs has no effect in the direct measurement of h . Because CNTs were the only dispersant to be used in our study, the use of particles of the other shapes could yield useful data for further discussion.

3.4 RHEOMETER SAMPLING DURATION

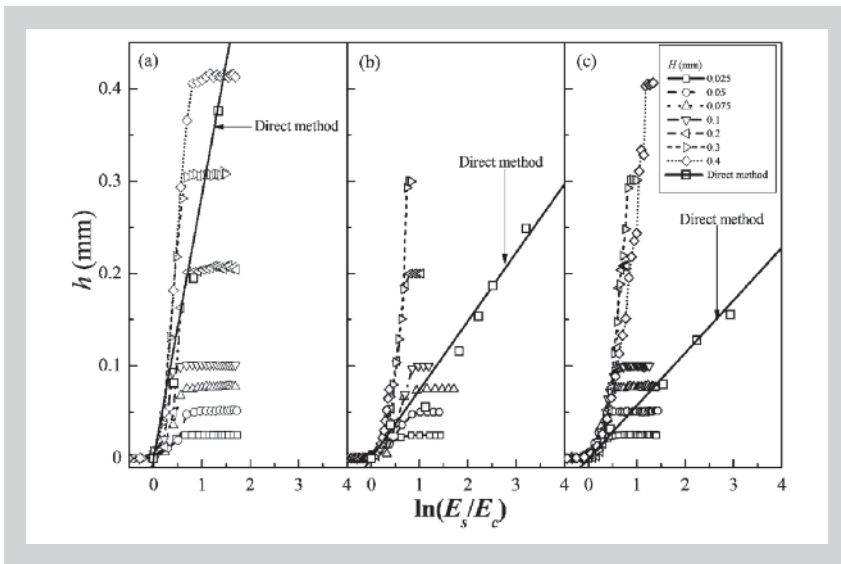
Because the solidification of the prepolymer was completed over a short time, our time-dependent rheological measurements had to be performed at a suitably fast sampling rate. This requirement was especially critical in the case of a small gap because the solidification was completed in a very short time. The appropriate sampling rate and duration may be deduced from the solidification characteristics of the photopolymer. The characteristic parameters for solidification are the critical exposure E_c and the depth of penetration D_p . The critical exposure $E_c = I_s \times T_c$ was obtained by measuring the critical exposure time T_c which was determined within the resolution of the sampling duration ΔT of the rheometer. In symbols $E_c \pm \Delta E_c = I_s \times (T_c \pm \Delta T)$ and

$$\frac{\Delta E_c}{E_c} = I_s \frac{\Delta T}{E_c} \quad (15)$$

In order to obtain a precise value for E_c , the surface light intensity I_s , or ΔT must be suitably small. The depth of penetration D_p is obtained from Equation 3 and $D_p \pm \Delta D_p = H \times \ln\{E_c/I_s(T_f \pm \Delta T)\}$ where T_f is the solidification time for a photopolymer of thickness H . Thus

$$\frac{\Delta D_p}{D_p} = -\ln\left(1 + \frac{\Delta T}{T_f}\right) \quad (16)$$

where T_f is given by $T_f = (E_c/I_s) \exp(H/D_p)$ from Equation 3. In order to obtain a precise value of



D_p , I_s or ΔT must be suitably small. A large value of H is also preferable in that this could help to reduce the error. However, in order to obtain the same results as from direct measurement, H should be less than 0.1 mm, as found from the measurements of unidirectional shear. When unidirectional flow was applied to the photopolymer without CNTs in this study, assuming $\Delta T = 0.08$ s, $T = 0.1$ mm, $I_s = 0.2$ mW/cm², $E_c = 0.3$ mJ/cm², and $D_p = 0.29$ mm, the estimated errors were $\Delta E_c/E_c \cong 5\%$ and $\Delta D_p/D_p \cong 4\%$. These errors are insignificant. However, the influence of sampling duration is severe in the dynamic measurements because $\Delta T = 1$ s (1 Hz). The estimated errors were $\Delta E_c/E_c \cong 67\%$ and $\Delta D_p/D_p \cong 39\%$. Therefore, either a shorter sampling duration, or a special customization, as applied by Schmidt et al. [14], is necessary when carrying out dynamic measurements. It should be noted that these errors could not explain the significant deviation from direct measurement seen in Figure 11.

3.5 VISCOSITY INCREASE BEFORE SOLIDIFICATION

Because the rate of photopolymerization is so fast, the pre-gel state was assumed to turn into the post-gel state instantaneously. The increase in viscosity prior to solidification was therefore neglected, and the initial viscosity was assumed to be preserved until solidification took place. This assumption of constant viscosity could introduce an element of disagreement in the results between the rheological and direct measurements. A more general analysis could also explain this disagreement. Here, we estimate the viscosity increase prior to solidification, and discuss its influence on the solidified depth h . As mentioned in the previous section, the dynamic measurements indicate more complicated solidification characteristics than the direct measurements do. For this reason, the viscosity increase is discussed only for unidirectional shear. In addition, our measurements are limited to the torque

moment, from which it is difficult to obtain the two unknowns of viscosity increase and solid layer thickness. The approximate determination of these unknowns may be possible by utilizing the characteristics of homogeneous solidification. For homogeneous chemical gelation, some studies have revealed a time-dependent change in viscosity. Apicella et al. [30] developed a single generalized relationship $\eta/\eta_1 = g(t/t_2)$ for epoxy resin in a temperature range of 50 - 180°C, where η_1 is the initial viscosity at a time t_1 , and t_2 is the critical time, at which an almost unlimited viscosity increase occurs in a parallel disk viscometer. The photopolymerization is dominated by exposure rather than time. We assume that a similar generalized relationship may pertain during photopolymerization, and that time t/t_2 may be replaced by exposure $e(x,t)/E_2$. The viscosity is assumed as follows

$$\frac{\eta(x,t)}{\eta_1} = g\left(\frac{e(x,t)}{E_2}\right) \quad (e(x,t) \leq E_2) \quad (17)$$

E_2 is the critical exposure that causes an almost unlimited viscosity increase, η_1 is the initial viscosity for $e(x,t) < E_2$, and E_1 is the exposure at which the viscosity increases. The effect of shear thinning in Equation 13 is neglected. Figure 16 shows a schematic representation of the changes in light intensity, exposure, and viscosity in the gap between the parallel disks. The constant viscosity assumed in Section 2.3 corresponds to $g = 1$. The case for $g \neq 1$ is discussed for the flow shown in Figure 16.

The flow between the parallel disks is axisymmetric, and the ratio of the disk distance H to the disk radius R is much less than 1. The continuity equation for this axisymmetric flow

$$\frac{1}{r} \frac{\partial(rv_r)}{\partial r} + \frac{\partial v_x}{\partial x} = 0 \quad (18)$$

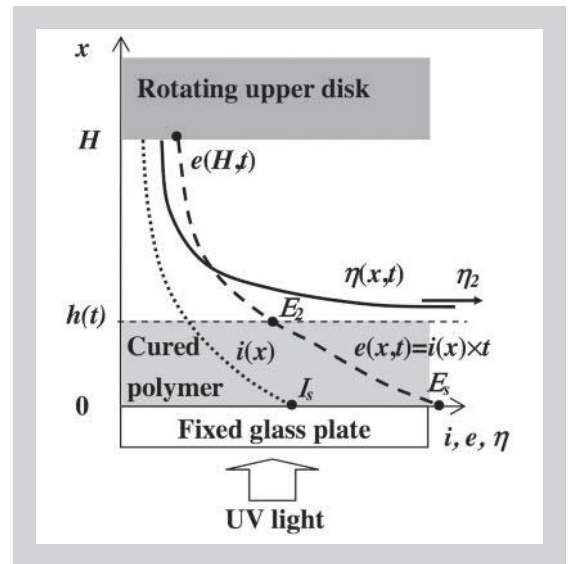


Figure 15 (left): Solidified depth h as a function of $\ln(E_s/E_c)$ for the dynamic measurements. The CNT concentration was 0% in (a), 0.05% in (b), and 0.1% in (c).

Figure 16: Depth-dependent changes in the light intensity i , exposure e , and viscosity η .

suggests that the order of v_x is $(H/R)xv_r$, and that v_x is therefore negligible in comparison with v_r . The continuity equation with $v_x = 0$ gives $v_r = 0$. From $v_x = v_r = 0$, the equation of motion may be reduced as follows

$$\frac{\partial}{\partial x} \left(\eta(x,t) \frac{\partial v_\theta}{\partial x} \right) + \eta(x,t) \frac{\partial}{\partial r} \left\{ r \frac{\partial}{\partial r} \left(\frac{v_\theta}{r} \right) \right\} = 0 \quad (19)$$

The inertial terms are neglected because of very small Reynolds number, the order of which is 10^{-4} to 10^{-3} . The following analysis includes integration and differentiation with respect to x , but not to t . Here, we separate the variables for a solution of v_θ

$$v_\theta = r\omega f\left(\frac{x}{H}\right) \quad (20)$$

The boundary conditions are defined as follows

$$\begin{aligned} v_\theta = 0, \quad f = 0 & \quad \text{at } x = h^* \\ v_\theta = r\omega, \quad f = 1 & \quad \text{at } x = H \end{aligned} \quad (21)$$

The solidified depth h^* is zero if the surface exposure $E_s(t) = I_s t$ at $x = 0$ is lower than the critical exposure E_2 . By integrating Equation 19 with respect to x , the function f may be obtained as follows

$$f'\left(\frac{x}{H}\right) = \frac{H}{g(e(x,t)/E_2)} \bigg/ \int_{h^*}^H \frac{dx}{g(e(x,t)/E_2)} \quad (22)$$

$$f\left(\frac{x}{H}\right) = 1 - \int_x^H \frac{dx}{g(e(x,t)/E_2)} \bigg/ \int_{h^*}^H \frac{dx}{g(e(x,t)/E_2)} \quad (23)$$

The torque moment on the disk is given by

$$M = \frac{\pi R^4 \omega \eta_1}{2} \bigg/ \int_{h^*}^H \frac{dx}{g(e(x,t)/E_2)} \quad (24)$$

where the wall shear rate is calculated on the upper disk from

$$\left(\frac{\partial v_\theta}{\partial x} \right)_{x=H} = \frac{r\omega}{H} f'(1) \quad (25)$$

By assuming that $\zeta(x,t) \equiv e(x,t)/E_2$

$$M = \frac{\pi R^4 \omega \eta_1}{2 D_p} \bigg/ \int_{\zeta(H,t)}^{\zeta(h^*,t)} \frac{d\zeta}{\zeta g(\zeta)} \quad (26)$$

where, $h^* = 0$ for $E_s(t)$ less than E_2 . In the simple case of $g = 1$, i.e., the viscosity is constant and fixed at η_1 , the moment is

$$M = \frac{\pi R^4 \omega \eta_1}{2(H-h^*)} = \frac{M_0}{1-h^*/H} \quad (27)$$

and is reduced to Equation 8 where $h^* = h$.

The exposure $e(x,t)$ decreases with penetration depth x and increases with time t , as given by Equation 2. However, there is no means of identifying the function $g(e(x,t)/E_2)$ from the measurement of torque moment. Otsubo et al. [9] discussed the effect of H when using an oscillating plate rheometer, and suggested that the viscosity increase may be homogeneous in a sample thickness of less than $10 \mu\text{m}$. This homogeneity of the viscosity may be explained in terms of the homogeneity of the exposure. When the gap is very small compared with D_p , the exposure $e(x,t) = I_s t / \exp(x/D_p)$ is more or less independent of the depth x . For example, a change in x from 0 to $25 \mu\text{m}$ corresponds to a change in $e(x,t)$ of $I_s t$ to $1.09 I_s t$ where D_p is assumed to be 0.29 mm (from Figure 6). $I_s t$ is equal to the surface exposure $E_s(t)$, and thus $g(e(x,t)/E_2) \cong g(E_s(t)/E_2)$ for a small gap. From this homogeneity for a small gap, we can predict $g(e(x,t)/E_2)$ as suggested by Otsubo et al. [9]. In other words, the function $g(E_s(t)/E_2)$ is determined from the results of a small gap and $E_s(t)/E_2$ in the obtained function $g(E_s(t)/E_2)$ is then replaced by $e(x,t)/E_2$. We apply this approach to predict the viscosity increase $g(e(x,t)/E_2)$ for the prepolymer without CNTs. The viscosity increase for $H = 25 \mu\text{m}$ is shown in Figure 8a from which the viscosity increase may be approximated by

$$g(\zeta) = \frac{1}{1 + \epsilon - \zeta^n} \quad (\zeta \leq 1) \quad (28)$$

where, $\zeta = E_s(t)/E_2$. The constants ϵ and n , obtained from Figure 8a, are 0.01 and 7, respectively. If $E_s(t) = E_2$ and therefore $\zeta = 1$, then $\eta/\eta_1 = g(1) = 1/\epsilon \gg 1$.

If $E_s(t) \leq E_1$ then $\eta/\eta_1 \cong 1$. The constant n is related to the magnitude of the range of ζ in which the viscosity increases. If n is large, the prepolymer increases in viscosity within a narrow range of ζ and is therefore rapidly solidified. In the next step, ζ is defined as $e(x,t)/E_2$ instead of $E_s(t)/E_2$ and Equations 26 and 28 are used to give the moment as follows

$$M = \frac{\pi R^4 \omega \eta_1}{2 D_p} \left\{ (1+\epsilon)(H-h^*) - \frac{1}{n+1} (\zeta(h^*,t)^{n+1} - \zeta(H,t)^{n+1}) \right\} \quad (29)$$

Thus

$$h^* = H \left(1 - \frac{M_o}{M} \right) - \Delta \quad (30)$$

where

$$\Delta = \frac{D_p}{(1+\epsilon)(n+1)} (\zeta(h^*,t)^{n+1} - \zeta(H,t)^{n+1}) \quad (31)$$

The first term in the denominator of Equation 29 is approximately $H - h^*$ because of $\epsilon \ll 1$, and indicates the liquid layer thickness. The second and third terms in the denominator indicate the contribution of increasing viscosity that occurs in the liquid layer from $x = h^*$ to $x = H$. Equation 31 includes the unknown values of solidified depth h^* in $\zeta(h^*,t)$ and depth of penetration D_p . However, the exposure $e(h^*,t)$ is E_2 and so $\zeta(h^*,t) = 1$. If $E_s(t)$ is lower than E_2 , $h^* = 0$, and $\zeta(h^*,t) = E_s(t)/E_2$. The depth of penetration D_p cannot be obtained because h^* is unknown in Equation 3. The solidified depth h obtained from Equation 8 is therefore used as the first approximation of h^* , thereby enabling D_p and Δ to be obtained in order that h^* may be calculated. As mentioned above, a large value of n in Equation 28 results in a rapid viscosity increase in a narrow range of ζ , and gives a small value for Δ in Equation 31. The method of characterization proposed in Section 2.3 corresponds to this limiting case of $n \gg 1$ and $\Delta \cong 0$. In Figure 10a, the solidified depth h^* calculated from Equation 30 is plotted with h calculated from Equation 8. The correction Δ is approximately 10 % of H . This modest degree of correction suggests that the rheological method in Section 2.3 can provide a reasonable set of values for the characterization of solidification.

The influence of shear on photopolymerization is important not only in rheological measurements, but also in applications such as coating. Further research must therefore be carried out in order to improve our understanding of the influence of shear on the photopolymerization reaction. Improvements, such as a combination with optical measurement, would make the rheological method more useful for the characterization of photopolymers.

3 CONCLUSIONS

The critical exposure E_c and the rate of change of solidified depth h were obtained from the results of rheological and direct measurements. In the analysis of solidification under unidirectional shear flow there were reasonable agreements on E_c and h with direct measurement when the sample thickness in the rheometer H was less than 0.1 mm. For H larger than 0.1 mm, the rheological method gave a higher critical exposure and a faster increase in h than direct measurement. In other words, when H was greater than 0.1 mm unidirectional shear initially delayed the start of the solidification and then caused it to occur more rapidly. This influence of H on solidification was more significant in dispersed systems of CNTs. On the other hand, for all values of H , dynamic measurements under oscillatory shear showed a significant difference in critical exposure and solidified depth from those values obtained by direct measurement.

ACKNOWLEDGMENT

The authors would like to express their sincere appreciation to Afit Corp. and Nikkiso Co., Ltd. for their donations of photopolymer and SWCNTs.

REFERENCES

- [1] Jacobs PF: Rapid Prototyping and Manufacturing: Fundamentals of Stereolithography, Society of Manufacturing Engineers (1992).
- [2] Schwalm R: UV coatings: Basic, recent developments and new applications, Elsevier Sci., Oxford, UK (2006).
- [3] Bauer F and Mehnert R: UV curable acrylate nanocomposites: properties and application, J. Polym. Res. 12 (2005) 483-491.
- [4] Iijima S: Helical microtubes of graphitic carbon, Nature 354 (1991) 56-58.
- [5] Moniruzzaman M and Winey KI: Polymer Nanocomposites Containing Carbon Nanotubes, Ma-

- cromolecules 39 (2006) 5194-5205.
- [6] Castel P, Wouters M, Fischer H, de With G: Kinetic study of UV-curable powder coating using photo-DSC, real-time FTIR and rheology, *J. Coat. Tech. Res.* 4 (2007) 411-423.
- [7] Watanabe K, Amari T, Otsubo Y, Dynamic viscoelastic measurement of photosensitive polymers, *J. App. Polym. Sci.* 29 (1984) 57-66.
- [8] Otsubo Y, Amari T, Watanabe K: Rheology behavior of epoxy acrylate prepolymer during UV curing, *J. App. Polym. Sci.* 29 (1984) 4071-4080.
- [9] Otsubo Y., T. Amari, K. Watanabe: Rheology studies of ultraviolet curing with an oscillating plate rheometer, *J. App. Polym. Sci.* 31 (1986) 323-332.
- [10] Khan SA, Plitz IM, and Frantz RA: In situ technique for monitoring the gelation of UV curable polymers, *Rheol. Acta* 31 (1992) 151-160.
- [11] Khan SA: Effect of shear on the gelation of UV-curable polymers, *J. Rheol* 36 (1992) 573-578.
- [12] Chiou BS, English RJ, and Khan SA: Rheology and photo-cross-linking of thiol-ene polymers, *Macromolecules* 29 (1996) 5368-5374.
- [13] Lee SS, Luciani A, Manson JAE: Rheological characterisation technique for fast UV-curable system, *Prog. Org. Coat.* 38 (2000) 193-197.
- [14] Schmidt LE, Leterrier Y, Vesin JM, Wilhelm M, and Manson JAE: Photorheology of fast UV-curing multifunctional acrylates, *Macromol. Mater. Eng.* 290 (2005) 1115-1124.
- [15] Tung CYM and Dynes PJ: Relationship between viscoelastic properties and gelation in thermosetting systems, *J. App. Polym. Sci.* 27 (1982) 569-574.
- [16] Winter HH and Chambon F: Analysis of linear viscoelasticity of a crosslinking polymer at the gel point, *J. Rheol.* 30 (1986) 387-382.
- [17] Winter HH: Can the gel point of a cross linking polymer be detected by G' - G'' crossover?, *Polym. Eng. Sci.* 27 (1987) 1698-1702.
- [18] Shaw MT and Liu ZZ: Single-point determination of nonlinear rheological data from parallel-plate torsional flow, *Appl. Rheol.* 16 (2006) 70-79.
- [19] Karchenko SB, Douglas JF, Obrzut J, Grulke EA, and Migler KB: Flow-induced properties of nanotube-filled polymer materials, *Nature Materials* 3 (2004) 564-569.
- [20] Rahatekar SS, Koziol KKK, Butler SA, Elliott JA, Shaffer MSP, Mackley MR, and Windle AH: Optical microstructure and viscosity enhancement for an epoxy resin matrix containing multiwall carbon nanotubes, *J. Rheol.* 50 (2006) 599-610.
- [21] Ma AWK, Chinesta F and Mackley MR: The rheology and modeling of chemically treated carbon nanotubes suspensions, *J. Rheol.* 53 (2009) 547-573.
- [22] Kinloch IA, Roberts SA, Windle AH: A rheological study of concentrated aqueous nanotube dispersions, *Polymer* 43 (2002) 7483-7491.
- [23] Fan Z and Advani SG: Rheology of multiwall carbon nanotube suspensions, *J. Rheol.* 51 (2007) 585-604.
- [24] Pötshke P, Fornes TD, Paul DR: Rheological behavior of multiwalled carbon nanotube/polycarbonate composites, *Polymer* 43 (2002) 3247-3255.
- [25] Ma AWK, Mackley MR, Chinesta F: The Microstructure and rheology of carbon nanotube suspension, *Int. J. Mater. Form.* 1 (2008) 75-81.
- [26] Andrzejewska E: Photopolymerization kinetics of multifunctional monomers, *Prog. Polym. Sci.* 26 (2001) 605-665.
- [27] Feng L and Suh BI: Exposure reciprocity law in photopolymerization of multi-functional acrylates and methacrylates, *Macromol. Chem. Phys.* 208 (2007) 295-306.
- [28] Vacche SD, Geiser V, Leterrier Y, and Manson JAE: Time-intensity superposition for photoinitiated polymerization of fluorinated and hyperbranched acrylate nanocomposites, *Polymer* 51 (2010) 334-341.
- [29] Pujari S, Rahatekar SS, Gilman JW, Koziol KK, Windle AH, and Burghardt WR: Orientation dynamics in multiwalled carbon nanotube dispersions under shear flow, *J. Chem. Phys.* 130 (2009) 214903.
- [30] Apicella A, Masi P, and Nicolais L: Rheological behavior of a commercial TGDDM-DDS based epoxy matrix during the isothermal cure, *Rheol. Acta* 23 (1984) 291-296.

